

Generalized Mosaicing: Polarization Panorama

Yoav Y. Schechner, *Member,
IEEE Computer Society*, and
Shree K. Nayar, *Member, IEEE*

Abstract—We present an approach to image the polarization state of object points in a wide field of view, while enhancing the radiometric dynamic range of imaging systems by generalizing image mosaicing. The approach is biologically-inspired, as it emulates spatially varying polarization sensitivity of some animals. In our method, a spatially varying polarization and attenuation filter is rigidly attached to a camera. As the system moves, it senses each scene point multiple times, each time filtering it through a different filter polarizing angle, polarizance, and transmittance. Polarization is an additional dimension of the generalized mosaicing paradigm, which has recently yielded high dynamic range images and multispectral images in a wide field of view using other kinds of filters. The image acquisition is as easy as in traditional image mosaics. The computational algorithm can easily handle nonideal polarization filters (partial polarizers), variable exposures, and saturation in a single framework. The resulting mosaic represents the polarization state at each scene point. Using data acquired by this method, we demonstrate attenuation and enhancement of specular reflections and semireflection separation in an image mosaic.

Index Terms—Mosaicing, color, image fusion, physics-based vision, illumination, transparent layers, biology-inspired.

1 INTRODUCTION

POLARIMETRIC imaging has been used in numerous imaging applications [23], [41], including object and material recognition [51], [52], shape recovery [30], [31], [50], and removal and analysis of specular reflections in photography and computer vision [14], [19], [24], [27], [39]. It has also been used for removal of scattering effects [11], [17], [46], e.g., in haze [35], underwater [9], [18], [33], [45], [52], and tissue [10]. The polarization state has four degrees of freedom, parameterized, for example, by the Stokes parameters. In nature, however, circular polarization is typically negligible [23], [42]. Thus, in this paper, we assume partial linear polarization, which is characterized by three parameters, i.e., the intensity, the degree of polarization, and the orientation of the plane of polarization (sometimes referred to as the phase angle). Nevertheless, this study can be extended to include elliptic polarization as well.

To recover the polarization parameters at each point, it is usually sufficient to measure the scene several times, each time with different polarization settings. Typically, this is achieved by filtering the light through a linear polarizer, oriented differently in different images. However, this is not the only way. In fact, biological systems use different mechanisms to capture polarization images. An eye considered as one of the most sophisticated with respect to polarization and color sensitivity is that of the mantis shrimp [7], [8]. Its retina has several distinct regions, each having different optical properties. In order to capture all the information in high quality, the shrimp moves its eyes to scan the field of view (FOV), thereby sequentially measuring each scene

point using different optical settings [7]. This gives the shrimp vision high quality color, polarization, and spatial information in a wide field of view.

Relative to the use of a static camera and a rotating polarizing filter, the benefit of the mantis shrimp eye is the ability to capture a wide FOV and, in addition, scan additional imaging dimensions (as wavelength). It is possible to incorporate this principle in man-made imaging systems using the approach of *generalized mosaicing*. In this approach, different portions of the camera FOV sense the scene in different optical settings. During acquisition of the image sequence, the camera moves, thereby capturing different portions of the scene. In postprocessing, the data extracted from these images is fused to create a wide FOV image mosaic. Most scene points in the resulting mosaic contain a wealth of information derived from the multiple settings in which they were captured.

Image mosaicing has long been used for a variety of fields, such as astronomy [47], remote sensing [48], and underwater research [13], [15], [28]. It has been used to obtain super-resolution [4], [43], capture wide FOV urban and indoor scenes [6], [20], [32], aid robot navigation [12], compress video [22], [26], and for virtual reality and 3D environmental information [29], [40], [44]. Its extension to generalized mosaics enabled the creation of high dynamic range (HDR) images [1], [36], [38] and multispectral images [36], [37]. Here, we exploit this approach to extract polarization information from the mosaicing process and, in addition, we extend the dynamic range.

We demonstrate this principle by attaching a spatially varying polarization filter in front of the camera. The computational algorithms tailored to this kind of a system handle, in a single framework, nonideal polarization filters (partial polarizers), variable exposures and saturation, in addition to system motion. As examples for applications, we use the extracted polarization information to analyze specular reflections.

2 EXTRACTING MEANINGFUL DATA

A given scene point is measured multiple times, each through a filter part with different characteristics and/or orientation. Some filter parts can be regarded as complete polarizers. Others are only partial polarizers. Moreover, the transmittance is also varying. If the measurements corresponding to the same scene point are registered, then polarization and HDR intensity information can be extracted. In this section, we gradually complicate the estimation method from the simple polarimetric equations to those we actually use.

Had the filter been an ideal polarizer oriented at an angle α , then the output of the polarizer would have been

$$i = [c + a \cos 2(\alpha - \theta)]/2, \quad (1)$$

where θ is the angle of the plane of polarization (phase angle), the degree of polarization is $p = a/c$, and the input intensity is c . Equation (1) can be rewritten as

$$i = 0.5 \cdot [1, \cos 2\alpha, \sin 2\alpha] \cdot [c, a^c, a^s], \quad (2)$$

where $a^c = a \cos 2\theta$ and $a^s = a \sin 2\theta$. In general, however, the polarizer is not ideal. Let the filter at measurement k have an average (unpolarized) transmittance of T_k . Let it partially polarize an unpolarized incident light to a degree P_k at angle α_k . Define $A_k^c = T_k P_k \cos 2\alpha_k$ and $A_k^s = T_k P_k \sin 2\alpha_k$. It can be easily shown that the output intensity is now

$$i_k = [T_k, A_k^c, A_k^s] \cdot [c, a^c, a^s], \quad (3)$$

in consistency with a derivation based on Stokes parameters [5].

2.1 Standard Polarization Estimation

To recover c , a^c , and a^s , at least three independent measurements are needed. When more than three are used, the least squares estimation is

• Y.Y. Schechner is with the Department of Electrical Engineering, Technion—Israel Institute of Technology, Haifa 32000, Israel. E-mail: yoav@ee.technion.ac.il.

• S.K. Nayar is with the Department of Computer Science, Columbia University, 1214 Amsterdam Ave., New York, NY 10027. E-mail: nayar@cs.columbia.edu.

Manuscript received 8 Jan. 2003; revised 11 Mar. 2004; accepted 18 Aug. 2004; published online 10 Feb. 2005.

Recommended for acceptance by R. Kumar.

For information on obtaining reprints of this article, please send e-mail to: tpami@computer.org, and reference IEEECS Log Number 118109.

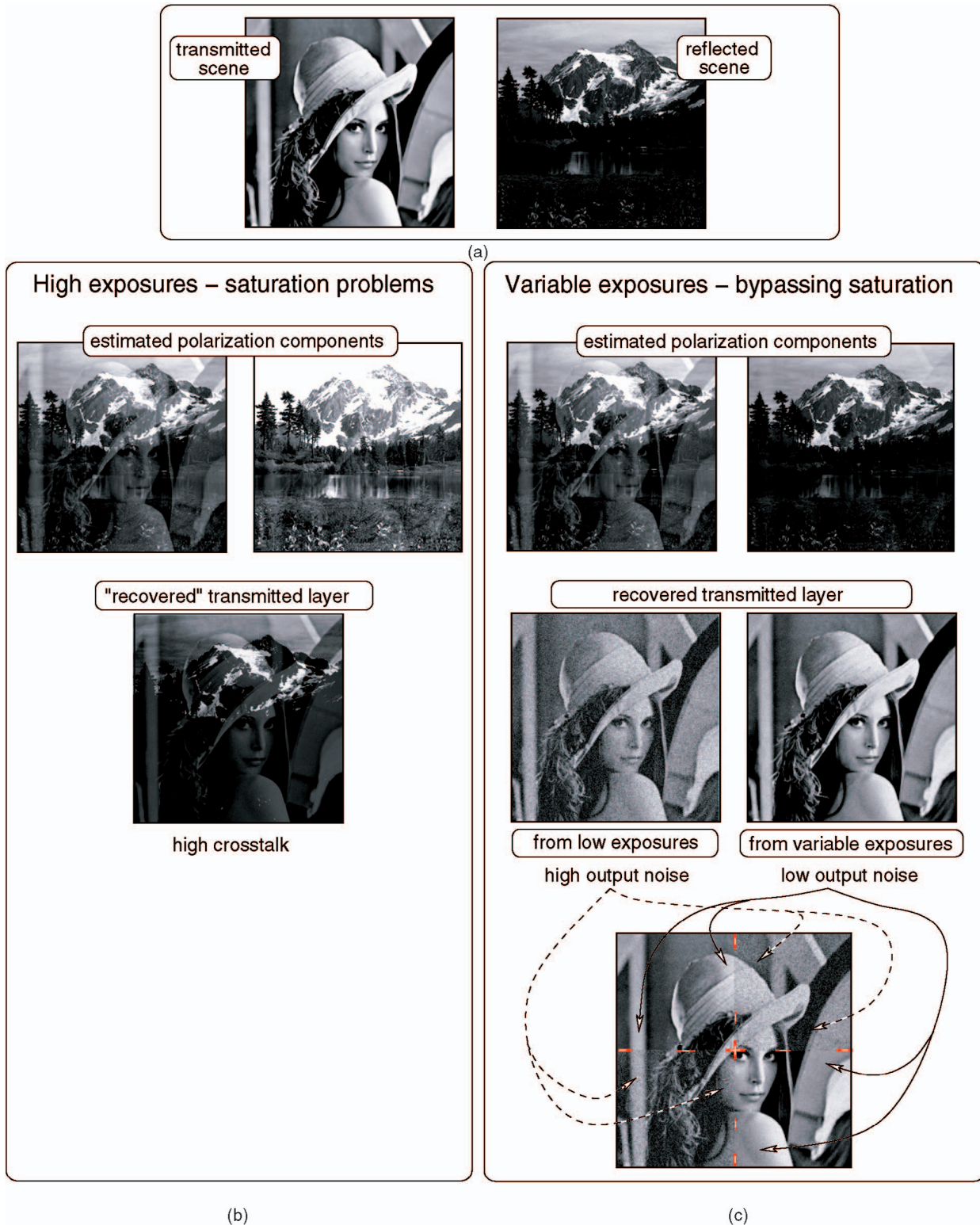


Fig. 1. Simulation. (a) A scene seen through a glass window and a scene semireflected by the window. (b) Attempting layer separation using high exposures of polarization filtered images leads to failure due to saturation. (c) Layers separation using low exposures increases noise. This noise is reduced and the contrast improves if variable exposures are used. In the bottom image, two quadrants were copied from the low noise result, while the other quadrants were copied from the high noise result. Their difference is noticed at the quadrant boundaries. For best comprehension, use the monitor to view these images.

$$[c, a^c, a^s]^t = (M^t M)^{-1} M^t \mathbf{i}, \quad (4)$$

where \mathbf{i} is the vector of intensity measurements and the rows of the matrix M are the filter's characteristic vectors at each measurement, $[T_k, A_k^c, A_k^s]$. This formalism is standard in polarization estimation.

2.2 Bypassing Saturation while Reducing Noise

The analysis in Section 2.1 ignores the effects of saturation in the raw images. When some of the measurements i_k are saturated, a significant error is induced into an estimation based on (4). Therefore, the estimated scene radiance and polarization parameters

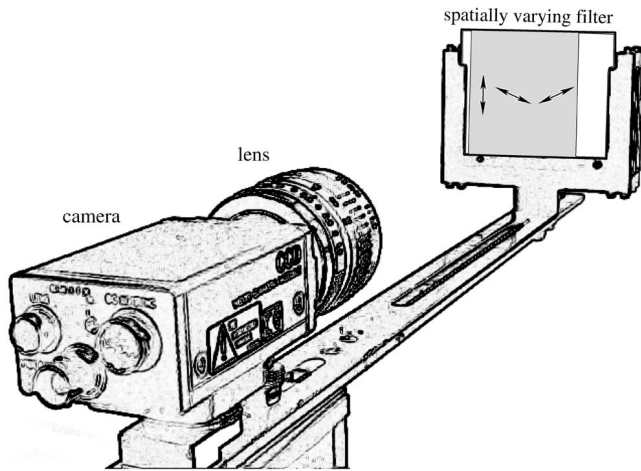


Fig. 2. A sketch of the system we used. A spatially varying polarizing filter is rigidly attached to the camera. The filter area includes clear (not filtering) segments to realize spatially varying attenuation as well.

strongly deviate from the true values. Such errors propagate to subsequent computer vision algorithms which exploit polarization.

As an example, consider a scene-layer semireflected from a glass window, through which a different scene layer is transmitted (Fig. 1). Viewing the combined scene through an ordinary polarizing filter yields different images, according to the orientation of the filter. High exposure settings saturate some pixels in some raw images. This leads to erroneous estimation of the polarization components of the measured light.¹ The parameters of these simulations are: angle of incidence is 35 degrees, 8-bit quantization; additive gaussian white noise (prior to quantization) with standard deviation of 1 gray-level; six raw frames are taken, two at each polarizer orientation of 0 degrees, 45 degrees, and 90 degrees.

The error in the estimation of polarization is apparent when using these components to separate the layers [39], as seen in Fig. 1b. That method exploits the fact that the different polarization components provide two independent superpositions of the two unknown layers. Using a physical model of the reflection, the image formation process is inverted [39], supposedly leading to layer separation. However, due to the nonlinear and irreversible nature of saturation, the estimated polarization components violate the superposition model.

Saturation is avoided if all the frames are taken in low exposure settings, e.g., using a neutral density filter. However, this leads to lower signal values relative to the measurement noise, e.g., due to quantization. Subsequently, the increased noise is propagated to the estimated polarization components and to the recovered scene layers, as simulated in Fig. 1c.

There is a way to bypass the saturation effects, while keeping the output noise low. It is based on using variable exposures. For instance, three of the six raw frames can be taken at a low exposure (one frame per polarizer angle), while the rest are taken at a high exposure. These measurements are combined using the method described in the next section. This algorithm yields a better result, shown in Fig. 1c: Most pixels have a low noise due to the high signals measured in the high exposures. On the other hand, saturated measurements do not ruin the calculations since they are backed up by low-exposure measurements. The results in this example more than doubled their signal to noise ratio (SNR), relative to the SNR obtained when all the images are taken in a low exposure.

1. The polarization components are parallel and perpendicular to the plane of incidence defined by the line of sight and the normal to the semireflecting window.

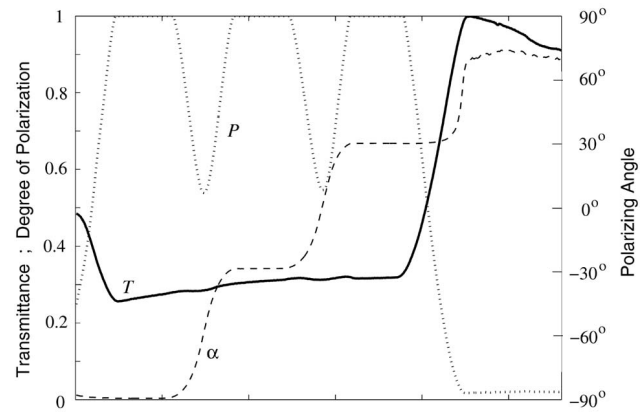


Fig. 3. (Solid) The spatially varying transmittance of the system. (Dotted) The spatially varying polarizance of the filter. (Dashed) The polarizing angle of the filter.

2.3 Variable Exposures (Transmittance) and Uncertainties

We adapt the standard estimation to process variable exposures. Consider the measurement $i_k \pm \Delta i_k$, where Δi_k is the uncertainty of a measurement. The uncertainty expresses saturation and camera nonlinearity. We term the raw image as g and the detector (nonlinear) radiometric response as R . Let the noise of the raw measurement be Δg . This noise is affected by photon shot noise, which originates from the signal itself. Noise is also caused by the

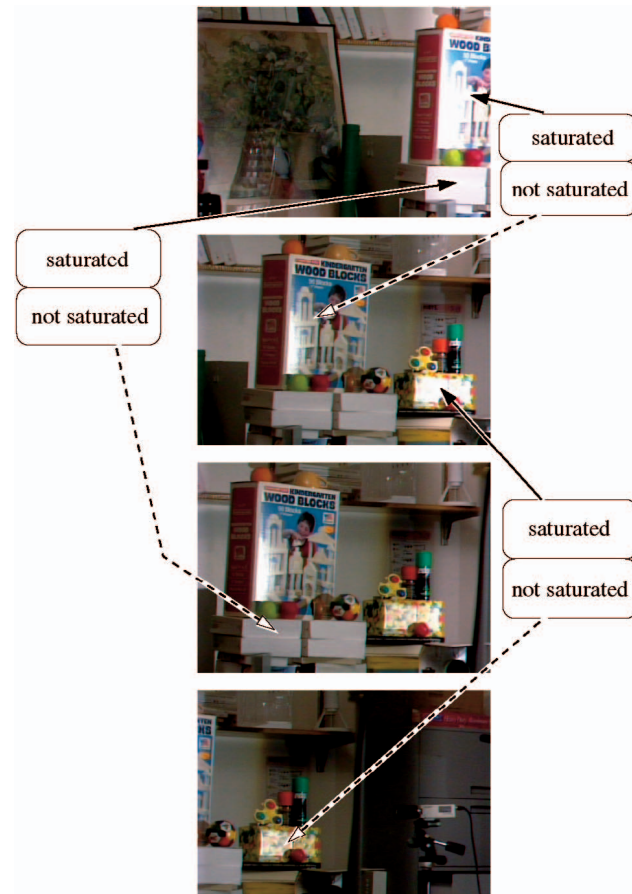


Fig. 4. A few frames from a sequence taken through the filter. The spatial variations of attenuation and polarization filtering are gradual and not easily visible due to the defocus blur of the filter. Nevertheless, this spatial variation makes objects appear brighter on the right-hand side. Thus, saturated pixels on the right appear unsaturated in their corresponding left-hand side pixels in other frames.



Fig. 5. The image mosaic rendered based on the frames acquired via the spatially varying filter. This is the image of the estimated unpolarized component c . The marked areas are analyzed as described in Section 5.3.

sensor. The sensor noise is dominant when using a standard 8-bit camera in daylight conditions. As a rough estimate for this noise, we set Δg to be the quantization error of the frame grabber (yet more elaborate figures can be used). Then,

$$i = R^{-1}(g), \quad \Delta i = \left| \frac{dR^{-1}(g)}{dg} \right| \Delta g. \quad (5)$$

For saturated pixels, we set $\Delta i \rightarrow \infty$.

To accommodate the uncertainty into the intensity and polarimetric measurements, we use a weighted least squares estimation:

$$[c, a^c, a^s]^t = (\mathbf{M}^t \mathbf{W} \mathbf{M})^{-1} \mathbf{M}^t \mathbf{W} \mathbf{i}, \quad (6)$$

where \mathbf{W} is a weighting diagonal matrix whose coefficients are $(\Delta i_k)^{-2}$. We note that, in [36], we derived the Maximum-Likelihood solution for fusing intensity measurements having different uncertainties which account for saturation and for varying attenuation. It can easily be shown that using $(\Delta i_k)^{-2}$ as weights makes (6) consistent with the prior results of [36] and actually generalizes these past results to handle polarization. One of the consequences of this method is that saturated measurements have a negligible weight relative to unsaturated ones.

3 SPATIALLY VARYING POLARIZER

We mount on the camera a filter which varies the polarization filtering across it, as depicted in Fig. 2. Due to defocus blur, the spatial variations are smoothed. In addition to the varying polarization filtering, the unpolarized attenuation also spatially varies in the system we use: the attenuation in some parts of the filter is stronger than in others. Now, let the scene be scanned by the rigid motion (e.g., lateral rotation) of the camera. The scene appears to move within the frame of the camera FOV. Due to the motion and the spatially varying filter, light coming from a given scene point is filtered differently at each frame. Therefore, mosaicing the frames enables polarization measurements of each scene point *while extending the FOV*.

In conjunction with the polarization estimation, the spatially varying transmittance enables the extension of the radiometric dynamic range. The reason is that scene points that are too dark to be reliably seen through the attenuating parts of the filter can be sensed more clearly through the transparent parts. On the other hand, scene points that are too bright can be saturated when viewed through the transparent portion while being unsaturated when viewed through the dark portions.

4 IMAGE REGISTRATION

A scene point has different coordinates in each image of the sequence. The measurements corresponding to this point should be identified before information is extracted from them. With generalized mosaicing, image registration is more challenging. The reason is that during motion, the image undergoes photometric transformations in addition to geometric ones. Several algorithms have been developed in the literature to handle such cases [2], [3],

[21], [25], [36], [49]. For lack of space, we direct the reader to these references for details.

In our example, we registered the images according to the approach we developed in [37], [38]. It generalizes the least squares difference image matching criterion by accounting for intensity measurement uncertainties. Note that inverting the attenuation of the filter amplifies the measurement noise. Hence, our image matching criterion [37], [38] uses a weighting similar to the one described in Section 2.3.

Imaging polarimetry implicitly involves subtraction of images. Therefore, misalignments cause significant errors at image edges, which can be apparent in subsequent computer vision algorithms exploiting polarization. We should note that errors in imaging polarimetry may also occur at image edges when using *static* cameras, as has been reported by several researchers [9], [27], [34], [51], [52]. That effect might have been caused by slight distortions created by the rotation of a fixed polarizer. We therefore expect that even a perfect registration will be prone to such a problem. As shown in [34], such problems are countered using *local alignments*. That procedure is similar to “deghosting” [40] techniques, which are standard in traditional image mosaicing.

5 EXPERIMENT

5.1 System Characteristics

In the system we used, the camera FOV was composed of several segments. In three segments, pieces of a polarizing sheet were placed² oriented at 60 degrees relative to one another. In the rest, light was freely transmitted (no filtering), as depicted in Fig. 2. The filter was attached to an NTSC camera via a rigid arm 20cm long. Due to defocus blur, the characteristics of the filter change gradually, rather than in steps. The effective transmittance of the system also changes due to lens vignetting and projection foreshortening. For these reasons, we precalibrated the transmittance and polarization filtering characteristics of the system. Prior to that, we had calibrated the system’s nonlinear radiometric response R using the MacBeth Chart [16]. We calibrated the filter characteristics by imaging a diffuse uniform target. In this calibration, a standard polarizer was rotated in front of the complete system.

Fig. 3 plots the system’s transmittance T , polarizance P , and polarizing angle α . The transmittance dynamic range is $\approx 1:4$. Thus, objects which are up to four times brighter than the unsaturated dynamic range of the camera can be viewed unsaturated through the filter. The three polarizing segments are identified by the regions for which $P = 1$, while the filter polarizance decreases between segments and at their periphery.

5.2 Mosaicing

We took a sequence of 37 still frames, samples of which are shown in Fig. 4. Note that objects are brighter (and even saturated) when they appear on the right-hand side of the frame. Then, we registered the images using the method mentioned in Section 4. The registration yielded a panoramic image mosaic, where the

2. We used off the shelf plastic polarizing sheets, which we attached to a thin glass substrate.

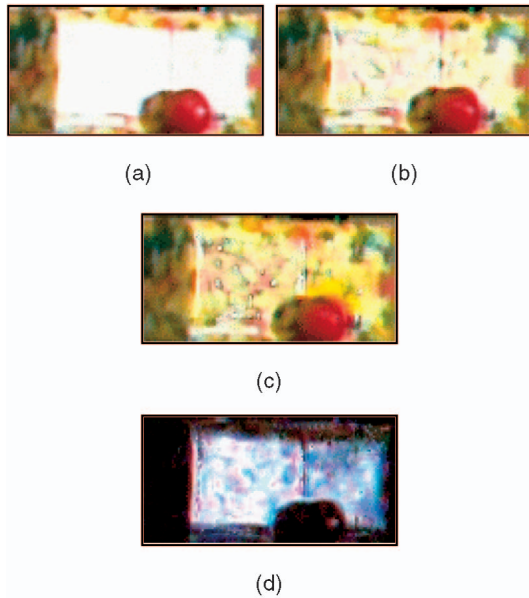


Fig. 6. Estimated images based on the raw data. (a) Enhancement of specularity by simulating imaging of the most intense polarization component. (b) Attenuation of specularity by simulating imaging of the least intense polarization component. (c) Recovered diffuse reflection. (d) Recovered specular reflection.

polarization is extracted at each point, using (6). We used feathering [40] to make the mosaic seamless. This was achieved by fading each frame towards its boundaries prior to the image fusion and polarization calculations.

From (6), we extracted the c component of the mosaic. This mosaic is shown in Fig. 5. Note that there are regions of saturation. High-intensity pixels are unsaturated through the polarizing segments and, indeed, their intensity is measurable. However, they are rendered saturated when simulating the unfiltered mosaic. The image registration was accurate since the mosaic is not blurred and all the details of the raw images appear in the mosaic of the c component.

5.3 Use of Polarization

Given the polarization information, we can analyze scene points and regions. We use polarization to run existing algorithms for analyzing specular reflections. Several scene regions are marked in Fig. 5. Consider the yellow box on the right. The specular reflection can be enhanced or attenuated by rendering the images $c + a$ and $c - a$, which correspond to the maximum and minimum intensities at each point when rotating a polarizer. These images are shown in Fig. 6a and Fig. 6b, respectively.³

Based on the *color* and the difference of these images, we applied the method described in [27] to separate the diffuse reflection component from the specular component. That method uses a dichromatic model. Pointwise subtraction of the minimum-intensity $c - a$ image from the maximum intensity $c + a$ image is associated with the 3D color *vector* of the specular highlights. Additional constraints are extracted from the color of neighboring pixels that reflect mainly diffusively [27]. The recovered components are shown in Fig. 6c and Fig. 6d, respectively. Fig. 7 shows a specular-enhanced bottle and also its recovered diffuse and specular components.

As another example, consider the glass-covered painting in the middle of the mosaic. The transparent cover semireflects a structure on the ceiling, making the painting unclear. Polarization imaging enables us to obtain somewhat different superpositions of

3. The resolution of the raw images is low. Thus, for display clarity, we magnified the corresponding estimated regions.

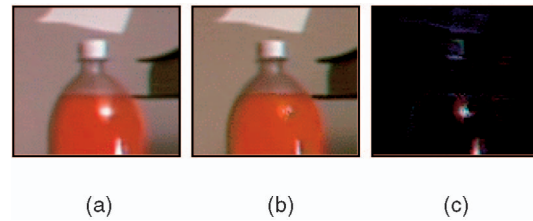


Fig. 7. Estimated images based on the raw data. (a) Enhancement of specularity by simulating the saturated imaging of the most intense polarization component. (b) Recovered diffuse reflection. (c) Recovered specular reflection.

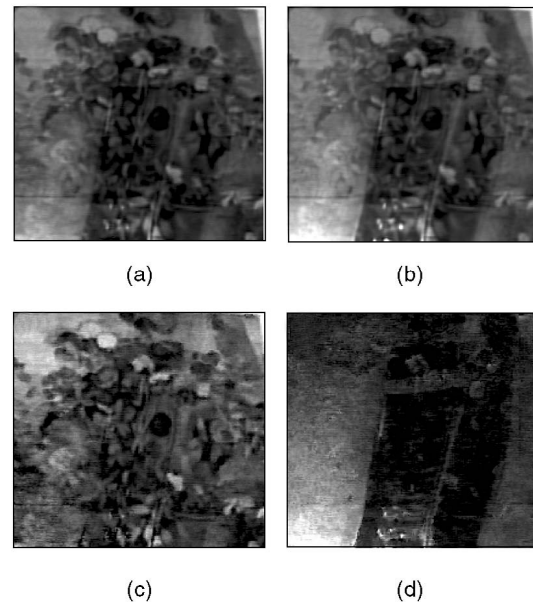


Fig. 8. Images of a glass covered painting. (a) The image corresponding to the polarization state parallel the plane of incidence. (b) The image corresponding to the polarization state perpendicular to the plane of incidence. (c) The recovered transmitted object. (d) The recovered reflected object.

the reflected scene (ceiling) and the transmitted scene (painting), as shown in Fig. 8a and Fig. 8b. These images correspond to the polarization components parallel or perpendicular to the plane of incidence (the line of sight and the surface normal). They were extracted from the mosaic.

Then, we applied the method of separating transparent and semireflected scenes, detailed in [39] and briefly described in Section 2.2. The method is based on an estimate of the angle of incidence.⁴ This estimate is obtained by computationally seeking a value for the incidence angle that minimizes the crosstalk of the estimated layers [39]. The layer crosstalk criterion is mutual information.

The estimated image of the reflection-free painting and image of the reflected structure are shown in Fig. 8c and Fig. 8d, respectively.

6 DISCUSSION

Generalized mosaicing is a framework for capturing enhanced scene information based on acquisition of a similar amount of data as in traditional mosaicing. We use this framework to compute high dynamic range and polarization images. This is in addition to previous work, in which we used the approach to obtain multispectral images. This approach has implications for several aspects of computer vision. It can be used in conjunction with

4. The angle of incidence is twice the angle between the line of sight and the normal to the glass cover.

current applications of mosaicing (e.g., remote sensing). It may also be used in conjunction with the wide range of applications of polarization imaging. As a by-product, we also derived an easy method for estimating polarization when the measurements include uncertainties, nonlinearities, saturation, and partial polarization filtering.

Dynamic scenes pose a problem to the method. If small objects move during the scene scan, then a conventional image mosaic can still be created. However, extracting polarization information about objects that move between measurements has not been treated in the literature yet. Therefore, we expect that obtaining polarization information about moving objects in the panorama FOV will be a difficult problem to solve.

ACKNOWLEDGMENTS

This work was supported in part by a US National Science Foundation ITR Award, IIS-00-85864, a David and Lucile Packard Fellowship, the US-Israel Binational Science Foundation (BSF), and the Ollendorff Minerva Center in the Electrical Engineering Department at the Technion. Minerva is funded through the BMBF. Yoav Schechner is a Landau Fellow, supported by the Taub Foundation, and an Alon Fellow.

REFERENCES

- [1] M. Aggarwal and N. Ahuja, "High Dynamic Range Panoramic Imaging," *Proc. IEEE Int'l Conf. Computer Vision*, vol. 1, pp. 2-9, July 2001.
- [2] F.M. Candocia, "Jointly Registering Images in Domain and Range by Piecewise Linear Comparometric Analysis," *IEEE Trans. Image Processing*, vol. 12, pp. 409-419, Apr. 2003.
- [3] F.M. Candocia, "Simultaneous Homographic and Comparometric Alignment of Multiple Exposure-Adjusted Pictures of the Same Scene," *IEEE Trans. Image Processing*, vol. 12, pp. 1458-1494, Dec. 2003.
- [4] D. Capel and A. Zisserman, "Automated Mosaicing with Super-Resolution Zoom," *Proc. IEEE Int'l Conf. Computer Vision and Pattern Recognition*, pp. 885-891, June 1998.
- [5] R.A. Chipman, "Polarimetry," *Handbook of Optics*, M. Bass, ed., second ed., vol. 2, chapter 22, New York: McGraw-Hill, 1995.
- [6] S. Coorg and S. Teller, "Spherical Mosaics with Quaternions and Dense Correlation," *Int'l J. Computer Vision*, vol. 37, pp. 259-273, June 2000.
- [7] T.W. Cronin and J. Marshall, "Parallel Processing and Image Analysis in the Eyes of the Mantis Shrimp," *Biology Bull.*, vol. 200, pp. 177-183, Apr. 2001.
- [8] T.W. Cronin, N. Shashar, R. Caldwell, J. Marshall, A.G. Cheroske, and T.H. Chiou, "Polarization Vision and Its Role in Biological Signaling," *Integrative and Comparative Biology*, vol. 43, pp. 549-558, Aug. 2003.
- [9] T.W. Cronin, N. Shashar, and L. Wolff, "Portable Imaging Polarimeters," *Proc. Int'l Conf. Pattern Recognition*, vol. 1, pp. 606-609, Oct. 1994.
- [10] S.G. Demos and R.R. Alfano, "Optical Polarization Imaging," *Applied Optics*, vol. 36, pp. 150-155, Jan. 1997.
- [11] L.J. Denes, M. Gottlieb, B. Kaminsky, and P. Metes, "AOTF Polarization Difference Imaging," *Proc. SPIE*, vol. 3584, pp. 106-115, 1999.
- [12] M. Eckmann and T.E. Boulton, "Tubular Mosaics [Path Planning]," *Proc. SPIE*, vol. 4195, pp. 192-203, 2001.
- [13] R. Eustice, O. Pizarro, H. Singh, and J. Howland, "UWIT: Underwater Image Toolbox for Optical Image Processing and Mosaicing in MATLAB," *Proc. IEEE Int'l Symp. Underwater Technology*, pp. 141-145, Apr. 2002.
- [14] H. Farid and E.H. Adelson, "Separating Reflections from Images by Use of Independent Component Analysis," *J. Optical Soc. Am. A*, vol. 16, no. 2136-2145, Sept. 1999.
- [15] R. Garcia, J. Battle, X. Cufi, and J. Amat, "Positioning an Underwater Vehicle through Image Mosaicing," *Proc. IEEE Int'l Conf. Robotics and Automation*, pp. 2779-2784, May 2001.
- [16] A.S. Glassner, *Principles of Digital Image Synthesis*, appendix G.4, Morgan-Kaufmann, 1995.
- [17] C.K. Harnett and H.G. Craighead, "Liquid-Crystal Micropolarizer Array for Polarization-Difference Imaging," *Applied Optics*, vol. 41, pp. 1291-1296, Mar. 2002.
- [18] S. Harsdorf, R. Reuter, and S. Tönebö, "Contrast-Enhanced Optical Imaging of Submersible Targets," *Proc. SPIE*, vol. 3821, pp. 378-383, 1999.
- [19] Hermanto, A.K. Barros, T. Yamamura, and N. Ohnishi, "Separating Virtual and Real Objects Using Independent Component Analysis," *IEICE Trans. Information and Systems*, vol. E84-D, no. 9, pp. 1241-1248, Sept. 2001.
- [20] S. Hsu, H.S. Sawhney, and R. Kumar, "Automated Mosaics via Topology Inference," *IEEE Computer Graphics and Application*, vol. 22, no. 2, pp. 44-54, Mar./Apr. 2002.
- [21] M. Irani and P. Anandan, "Robust Multi-Sensor Image Alignment," *Proc. IEEE Int'l Conf. Computer Vision*, pp. 959-966, Jan. 1998.
- [22] M. Irani, P. Anandan, J. Bergen, R. Kumar, and S. Hsu, "Efficient Representations of Video Sequences and Their Application," *Signal Processing: Image Comm.*, vol. 8, pp. 327-351, May 1996.
- [23] G.P. Können, *Polarized Light in Nature*. Cambridge Univ. Press, 1985.
- [24] S. Lin and S.W. Lee, "Detection of Specularity Using Stereo in Color and Polarization Space," *Computer Vision and Image Understanding*, vol. 65, pp. 336-346, Feb. 1997.
- [25] S. Mann, "Joint Parameter Estimation in Both Domain and Range of Functions in Same Orbit of the Projective-Wyckoff Group," *Proc. IEEE Int'l Conf. Image Processing*, pp. 193-196, Sept. 1996.
- [26] H. Nicolas, "New Methods for Dynamic Mosaicing," *IEEE Trans. Image Processing*, vol. 10, pp. 1239-1251, Aug. 2001.
- [27] S.K. Nayar, X.S. Fang, and T. Boulton, "Separation of Reflection Components Using Color and Polarization," *Int'l J. Computer Vision*, vol. 21, pp. 163-186, Feb. 1997.
- [28] S. Negahdaripour, X. Xu, A. Khemene, and Z. Awan, "3-D Motion and Depth Estimation from Sea-Floor Images for Mosaic-Based Station-Keeping and Navigation of ROV's/AUV's and High-Resolution Sea-Floor Mapping," *Proc. IEEE Workshop Autonomous Underwater Vehicles*, pp. 191-200, Aug. 1998.
- [29] S. Peleg, M. Ben-Ezra, and Y. Pritch, "Omnistereo: Panoramic Stereo Imaging," *IEEE Trans. Pattern Analysis and Machine Intelligence*, vol. 23, no. 3, pp. 279-290, Mar. 2001.
- [30] S. Rahmann and N. Canterakis, "Reconstruction of Specular Surfaces Using Polarization Imaging," *Proc. IEEE Int'l Conf. Computer Vision and Pattern Recognition*, vol. 1, pp. 149-155, Dec. 2001.
- [31] M. Saito, Y. Sato, K. Ikeuchi, and H. Kashiwagi, "Measurement of Surface Orientations of Transparent Objects by Use of Polarization in Highlight," *J. Optical Soc. Am. A*, vol. 16, pp. 2286-2293, Sept. 1999.
- [32] H.S. Sawhney, R. Kumar, G. Gendel, J. Bergen, D. Dixon, and V. Paragano, "VideoBrush: Experiences with Consumer Video Mosaicing," *Proc. IEEE Workshop Applications of Computer Vision*, pp. 52-62, Oct. 1998.
- [33] Y.Y. Schechner and N. Karpel, "Clear Underwater Vision," *Proc. IEEE Int'l Conf. Computer Vision and Pattern Recognition*, vol. 1, pp. 536-543, June 2004.
- [34] Y.Y. Schechner, N. Kiryati, and J. Shamir, "Separation of Transparent Layers by Polarization Analysis," *Proc. Scandinavian Conf. Image Analysis*, vol. 1, pp. 235-242, June 1999.
- [35] Y.Y. Schechner, S.G. Narasimhan, and S.K. Nayar, "Instant Dehazing of Images Using Polarization," *Proc. IEEE Int'l Conf. Computer Vision and Pattern Recognition*, vol. 1, pp. 325-332, Dec. 2001.
- [36] Y.Y. Schechner and S.K. Nayar, "Generalized Mosaicing," *Proc. IEEE Int'l Conf. Computer Vision*, vol. 1, pp. 17-24, July 2001.
- [37] Y.Y. Schechner and S.K. Nayar, "Generalized Mosaicing: Wide Field of View Multispectral Imaging," *IEEE Trans. Pattern Analysis and Machine Intelligence*, vol. 24, no. 10, pp. 1334-1348, Oct. 2002.
- [38] Y.Y. Schechner and S.K. Nayar, "Generalized Mosaicing: High Dynamic Range in a Wide Field of View," *Int'l J. Computer Vision*, vol. 53, pp. 245-267, Aug. 2003.
- [39] Y.Y. Schechner, J. Shamir, and N. Kiryati, "Polarization and Statistical Analysis of Scenes Containing a Semireflector," *J. Optical Soc. Am. A*, vol. 17, pp. 276-284, Feb. 2000.
- [40] H.Y. Shum and R. Szeliski, "Systems and Experiment Paper: Construction of Panoramic Image Mosaics with Global and Local Alignment," *Int'l J. Computer Vision*, vol. 36, pp. 101-130, Feb. 2000.
- [41] W.A. Shurcliff and S.S. Ballard, *Polarized Light*. D. van Nostrand Co., 1964.
- [42] A.M. Shutov, "Videopolarimeters," *Soviet J. Optical Technology*, vol. 60, pp. 295-301, May 1993.
- [43] A. Smolic and T. Wiegand, "High-Resolution Image Mosaicing," *Proc. IEEE Int'l Conf. Image Processing*, vol. 3, pp. 872-875, Oct. 2001.
- [44] R. Szeliski, "Image Mosaicing for Telepresence Applications," *Proc. IEEE Workshop Applications of Computer Vision*, pp. 44-53, Dec. 1994.
- [45] J.S. Talyor Jr. and L.B. Wolff, "Partial Polarization Signature Results from the Field Testing of the Shallow Water Real-Time Imaging Polarimeter (SHRIMP)," *MTS/IEEE Oceans*, vol. 1, pp. 107-116, Nov. 2001.
- [46] J.S. Tyo, M.P. Rowe, E.N. Pugh Jr., and N. Engheta, "Target Detection in Optically Scattering Media by Polarization-Difference Imaging," *Applied Optics*, vol. 35, pp. 1855-1870, Apr. 1996.
- [47] J.M. Uson, S.P. Boughn, and J.R. Kuhn, "The Central Galaxy in Abell 2029: An Old Supergiant," *Science*, vol. 250, pp. 539-540, Oct. 1990.
- [48] A.R. Vasavada, A.P. Ingersoll, D. Banfield, M. Bell, P.J. Gierasch, and M.J.S. Belton, "Galileo Imaging of Jupiter's Atmosphere: The Great Red Spot, Equatorial Region, and White Ovals," *Icarus*, vol. 135, no. 265-275, Sept. 1998.
- [49] P. Viola and W.M. Wells III, "Alignment by Maximization of Mutual Information," *Int'l J. Computer Vision*, vol. 24, pp. 137-154, Sept. 1997.
- [50] A.M. Wallace, B. Laing, E. Trucco, and J. Clark, "Improving Depth Image Acquisition Using Polarized Light," *Int'l J. Computer Vision*, vol. 32, pp. 87-109, Sept. 1999.
- [51] L.B. Wolff, "Polarization Camera for Computer Vision with a Beam Splitter," *J. Optical Soc. Am. A*, vol. 11, no. 11, pp. 2935-2945, Nov. 1994.
- [52] L.B. Wolff, "Polarization Vision: A New Sensory Approach to Image Understanding," *Image and Vision Computing*, vol. 15, pp. 81-93, Feb. 1997.